Royston, S., Bingham, R. J., & Bamber, J. L. (2022). Attributing decadal climate variability in coastal sea-level trends. *Ocean Science*, *18*(4), 1093-1107. https://doi.org/10.5194/os-18-1093-2022

University of Bristol - Explore Bristol Research
General rights

Ocean Science

Attributing decadal climate variability in coastal sea-level trends

Sam Royston[1], **Rory J. Bingham**[1], and **Jonathan L. Bamber**[1,2]

[1]School of Geographical Sciences, University of Bristol, Bristol, UK
[2]AI4EO, Technical University Munich, Munich, Germany

Correspondence: Sam Royston (s.royston@bristol.ac.uk)

Abstract. Decadal sea-level variability masks longer-term changes due to natural and anthropogenic drivers in short-duration records and increases uncertainty in trend and acceleration estimates. When making regional coastal management and adaptation decisions, it is important to understand the drivers of these changes to account for periods of reduced or enhanced sea-level change. The variance in decadal sea-level trends about the global mean is quantified and mapped around the global coastlines of the Atlantic, Pacific, and Indian oceans from historical CMIP6 runs and a high-resolution ocean model forced by reanalysis data. We reconstruct coastal, sea-level trends via linear relationships with climate mode and oceanographic indices. Using this approach, more than one-third of the variability in decadal sea-level trends can be explained by climate indices at 24.6 % to 73.1 % of grid cells located within 25 km of a coast in the Atlantic, Pacific, and Indian oceans. At 10.9 % of the world's coastline, climate variability explains over two-thirds of the decadal sea-level trend. By investigating the steric, manometric, and gravitational components of sea-level trend independently, it is apparent that much of the coastal ocean variability is dominated by the manometric signal, the consequence of the open-ocean steric signal propagating onto the continental shelf. Additionally, decadal variability in the gravitational, rotational, and solid-Earth deformation (GRD) signal should not be ignored in the total. There are locations such as the Persian Gulf and African west coast where decadal sea-level variability is historically small that are susceptible to future changes in hydrology and/or ice mass changes that drive intensified regional GRD sea-level change above the global mean. The magnitude of variance explainable by climate modes quantified in this study indicates an enhanced uncertainty in projections of short- to mid-term regional sea-level trend.

1 Introduction

Sea-level variability at the coast is driven by a variety of global- to local-scale factors. Understanding the drivers of variability due to decadal-scale climate variability in historical and contemporary observations improves our understanding of sea-level change and enhances our ability to predict future, near-term sea-level change. By subtracting climate-driven sea level from observations, a more consistent global mean sea level can be obtained from altimetry (Nerem et al., 2018) and tide gauge data (Frederikse et al., 2018). One aim is to elucidate anthropogenically driven sea-level change from climate variability (Hamlington et al., 2014, 2019). When climate variability can be explained, by reducing both the magnitude and auto-regressive nature of variability in the signal, the linear trend and acceleration standard errors can be reduced. This has been successfully applied globally (e.g. Hamlington et al., 2013; Nerem et al., 2018; Hamlington et al., 2020c) and regionally from climate variability dominated by atmosphere–ocean interactions (e.g. Zhang and Church, 2012; Pfeffer et al., 2018; Richter et al., 2020; Hamlington et al., 2020b; Wang et al., 2021; Pfeffer et al., 2022) and intrinsic, oceanic variability in eddy-rich regions (Sérazin et al., 2016). Understanding the driving mechanisms behind local, decadal sea-level change could lead to improved short- to medium-term forecasts of coastal sea-level change.

Regional sea level is projected to vary by 30 % from the global mean according to climate model evaluations (IPCC, 2019). Spatial patterns in sea-level variability are driven by intrinsic and climate variability as well as anthropogenic forcing and their interactions, resulting in intensified sea-level change by region (as demonstrated by climate models with historical forcing; Fasullo and Nerem, 2018). In

particular, changes to ocean heat content and surface winds drive changes in ocean circulation, in turn affecting the location of fronts and mixed layer or thermocline depth, which induce a sea-level change (e.g. Fasullo and Nerem, 2018; Fasullo et al., 2020; Peyser et al., 2016; Richter et al., 2020). Also, variations to the gravitational, rotational, and deformational (GRD) equipotential redistribute the sea surface, following anthropogenically forced mass redistribution such as dam impoundment, groundwater extraction, or anthropogenically driven ice mass loss (Wada et al., 2017; Meyssignac et al., 2017; Frederikse et al., 2020b). The remainder of the regional variation we describe hereafter as atmospheric and/or oceanic "internal" variability. Hereafter, we will use the terms "intrinsic variability" and "climate variability" to describe and differentiate these sources of variability. By intrinsic variability we mean the oceanic variability that is not driven by atmospheric forcing but is internal. We use climate variability to refer to atmospheric–oceanic variability intrinsic to the climate system, not driven by anthropogenic forcing. Local sea-level trends greater than $10\,\mathrm{mm\,yr^{-1}}$ on 10-year timescales and over $1\,\mathrm{mm\,yr^{-1}}$ on 30-year timescales are observed in areas of the Pacific Ocean driven by climate variability; climate variability may potentially contribute centimetres of sea-level change over any given 10-year period, which local planners and stakeholders need to account for (Hamlington et al., 2020a). This climate variability may affect the magnitude of regional sea-level trends calculated over durations up to 50 years (Carson et al., 2015, 2019). Sea-level variability related (linearly) to climate indices shows larger correlation coefficients at coastal locations in tide gauge data than in open-ocean altimetry (Wang et al., 2021). Statistically significant relationships between the steric and manometric components of sea level and climate variability have been identified from models, reanalyses, and geodetic observations (Pfeffer et al., 2018, 2022). These works validate model and reanalyses data sets for sea-level studies and identify regions of the global ocean with explainable, climate-driven, inter-annual to decadal variability, masking anthropogenically driven changes and modifying coastal flood risk about the long-term trend on decadal periods.

Decadal variability in global mean sea level is dominated by the El Niño–Southern Oscillation (ENSO) and Pacific Decadal Oscillation (PDO) and their evolution in time (Hamlington et al., 2013; Nerem et al., 2018; Hamlington et al., 2020c). Because these signals are large and affect a large proportion of the global ocean area (being equatorial–tropical), they dominate the global signal. But other climate processes, described by other major indices, of course also affect local sea-level variability (Woodworth et al., 2019).

The Pacific Ocean decadal sea-level variability is dominated by the ENSO and PDO processes (e.g. Zhang and Church, 2012; Hamlington et al., 2019). Additionally, the Southern Annular Mode (SAM) and Indian Ocean Dipole (IOD) can also be related to sea-level variability in the Pa-

cific Ocean (e.g. Frankcombe et al., 2015). The IOD covaries with ENSO on inter-annual timescales; via atmospheric tele-connections the IOD affects equatorial wind anomalies, and Pacific Ocean sea-level anomalies may transit through the Indonesian throughflow. The relationship is weaker at decadal timescales, but a significant correlation remains (Nidheesh et al., 2019). The IOD dominates sea-level variability in the Indian Ocean (Nidheesh et al., 2019). In the North Atlantic Ocean and North Sea, variability can be related to the North Atlantic Oscillation (NAO) and East Atlantic Pattern (e.g. Frederikse et al., 2018; Kleinherenbrink et al., 2016). We extend these analyses by focusing only on coastal sea level, and we remove the global mean sea level at each time step to investigate regional, spatial differences.

Although the spatial variability of regional, decadal-scale sea-level trends is dominated by the steric component (Richter et al., 2020), manometric sea-level changes dominate variability at the coast (Penduff et al., 2019; Llovel et al., 2018). When a steric-driven disturbance in the open-ocean sea surface height nears a coast, the density-driven change over a shallowing water column cannot fully match that in the open ocean and a pressure gradient develops in the sea surface. The geostrophic balance is maintained by redistribution of mass onto the shelf such that sea-level change at the coast exhibits a predominantly manometric signal (Landerer et al., 2007; Yin et al., 2010; Bingham and Hughes, 2012; Penduff et al., 2019). We therefore also investigate the components of sea-level variability at the coast.

Here we use a 53-year run of a high-resolution ocean model to quantify and characterise decadal-scale sea-level trend variability at the local, coastal scale (with the global mean removed). A comparison is made with the CMIP6 historical run ensemble mean and spread. Climate model runs will not, in general, mimic the timing of internal atmosphere–ocean variability correctly but should capture much of its magnitude in the ensemble spread. Observed regional variability can be greater than coarse models suggest (Meyssignac et al., 2017; Carson et al., 2019); hence, we compare the high-resolution run with the CMIP6 ensemble. These model runs are computationally expensive and we discuss the potential to use the relationship between sea-level variability and climate indices. We project climate mode indices onto the leading principal components (PCs) of an empirical orthogonal function (EOF) decomposition to reconstruct decadal, coastal sea-level trends associated with climate variability. With our focus at the coast, the reconstruction is applied to satellite altimetry and tide gauge observations, and the variability of coastal sea-level trends is discussed.

2 Method

Although ENSO variability dominates the spatial pattern of sea-level variability on decadal timescales, we wish to in-

vestigate if particular climate processes dominate sea-level trends, at the coast, over different regions, and for each component of sea-level change.

Climate and high-resolution ocean model runs are used to quantify the variability in decadal sea-level trends at the coast from each component part. A reconstruction of coastal, decadal sea-level trends using only standard climate mode indices is attempted that can be easily replicated by projecting climate mode indices onto PCs of decadal, coastal sea-level trends. Variability of the coastal, decadal trends in sea-level components (derived from the high-resolution ocean model sea-level components plus GRD) is characterised by an EOF analysis for each major ocean basin. The PCs of these sea-level component modes are correlated against climate mode indices to identify if a climate mode index covaries with any PC (of each sea-level component and in each ocean basin). For each sea-level PC in terms of diminishing variance explained (per component and basin), the climate index with maximum correlation is projected onto a PC by a linear regression until each climate index is used or the correlation is not statistically significant. Thus, the decadal sea-level variability that can be associated with climate variability is reconstructed by one climate index and regression coefficient for each EOF–PC mode, with the sum over reconstructed PCs giving the total sea-level variability.

Firstly, the magnitude of variance in regional sea level and its trend are determined from ocean models. These variances are calculated for total sea level and its component parts of manometric (model ocean bottom pressure) and steric contributions, plus the gravitation, rotation, and solid-Earth deformation response (GRD) contribution from the deviation from the global mean at each time step (refer to Gregory et al., 2019, for terminology).

We use output from a high-resolution (nominally 1/12°), eddy-resolving ocean model (NEMO) run over 58 years at monthly resolution from 1958–2015, in which the component steric and manometric signals sum to the sea-level signal (Marzocchi et al., 2015; Moat et al., 2016). We use the later 53 years of data, allowing for 5 years of spin-up. The global mean sea level is removed at each time step, since we are primarily interested in the regional variability about the mean. The "zos" variable for sea level does not include atmospheric pressure effects and is therefore not included in this assessment. Thus, the processed sea level quantifies the direction and variability of spatial patterns and intensification in sea level caused by observed atmospheric forcing plus intrinsic oceanic variability, excluding the inverse barometer effect. It is acknowledged that this variability will include influence from anthropogenic sources because the high-resolution model is forced by reanalysis atmospheric data rather than natural forcing. The magnitude of variability is compared against the ensemble mean and spread of variance for the same time period from an ensemble of 43 historical forcing CMIP6 models.

The observed absolute sea-level signal as observed by altimetry includes the GRD component that is spatially varying. The barystatic, global ocean mean volume change due to solid-Earth deformation is ignored in this study because we remove the global mean at each time step. We add only the spatial geoid signal to the sea surface height (SSH) from the models (with a global ocean mean of zero).

To quantify how much of the sea-level variability can be described by a relationship with climate indices, where the impact of sea-level change is highest – at the coast – we investigate reconstructing sea level from climate indices over a decadal timescale. We investigated both low-pass-filtered and rolling linear trends in time for each coastal grid cell time series and found the strongest relationship in the latter (not shown). We assume first-order auto-regressive (AR1) noise, appropriate for monthly sea-level time series (e.g. Bos et al., 2013; Dangendorf et al., 2014; Haigh et al., 2014), by a generalised least-squares regression that solves for the annual and semi-annual periodics as well as the trend. We apply an EOF analysis to the rolling decadal trends from the modelled component parts and compare against decadal trends in key climate indices.

It is acknowledged that there are limitations in using EOF analysis and a linear regression to associate climate variability with sea-level variability. Of course, the EOF method identifies the largest variance for its leading mode, and each mode is orthogonal from that. Therefore, even when care is taken to deseason and detrend the coastal, sea-level component time series, variability from specific physical drivers may be distributed into several EOF–PC modes. However, by reducing the spatial dimensions using EOF analysis we limit computational effort and redundancy in the analysis because of spatial covariance and produce a small data set of EOF patterns and loadings with just one set of regression coefficients each.

To focus on where the impact of sea-level change is highest and because the EOF analysis determines orthogonal bases from the first PC with the largest variability, we only apply the analysis to coastal regions. We define coastal by distance to the nearest coastline, selecting those model grid centres less than 25 km of distance from one of the low-resolution coastlines in the global self-consistent, hierarchical, high-resolution geography (GSHHG) database (following Penduff et al., 2019).

Our aim is to relate climate mode indices with the sea-level variability EOFs. A multivariate linear regression analysis could be used. Linear regression analysis only finds the analytical least-square error fit in the case of Gaussian data (no auto-correlation in the time series) and with independent explanatory variables. Some studies have reduced the impact of multicollinearity of the explanatory variables by low-pass and high-pass filtering correlated climate indices, giving new indices that represent short- and long-timescale processes (e.g. Zhang and Church, 2012; Wang et al., 2021). Alternatively, the inflation of regression coefficients due to

multicollinearity of the explanatory variables may be reduced by the use of a penalty or regularisation term, i.e. a ridge regression. A least absolute shrinkage and selection operator (LASSO) regression approach has been successfully applied to steric sea-level change (Pfeffer et al., 2018) and ocean mass change (Pfeffer et al., 2022) associated with climate variability on inter-annual and longer timescales. This approach relies on the user determining an appropriate penalty term, typically by a cross-validation.

We take a simpler approach that does not have tunable parameters. For the reconstruction, we rank all leading EOFs and retain those that describe at least 5 % of the sea-level trend variability for each component of sea-level change. For each leading PC in turn, a linear regression is applied to the climate index with the highest correlation coefficient, provided the correlation is significant (by t test with the degrees of freedom reduced due to the auto-regressive nature of the signal; Emery and Thomson, 2001). This approach capitalises on the orthogonality of the sea-level trend PCs and ensures each climate mode index is only used once and only when significant. The reconstruction sums the climate index multiplied by the regression coefficient for each climate index–PC pair until all climate modes are used and/or the correlation is not significant against any PC. However, as the EOF analysis may split the variability from a given physical process into more than one mode, it is likely that the relationship between a single climate index and single PC will underestimate the total variance caused by climate variability. Thus, the reconstructed climate-associated sea-level trends produced should be thought of as a lower limit at each location of the trend variance about the mean trend.

Reconstructed trends are compared against the variability of running trends from the model, giving the variance explained by the climate index regression, calculated as the percentage ratio of trend variance at each grid cell, of the model-minus-reconstructed residual over the model rolling trends. The variance explained by these reconstructions of course varies by the adequacy of a simple linear model and the number of leading principal component modes used in the reconstruction.

To validate our method, an example period of satellite altimetry data from 2008–2018 is taken. We compare the reconstruction for the trend from 2008–2018 against observed sea level from satellite altimetry. The reconstruction for running trends centred on 1968–2011 is compared against tide gauge observations at arbitrary locations, demonstrating locations where the variance explained appears to be good. The decadal trend variability from tide gauge observations and the reduction in variability explained by all significant PCs are determined for manometric, GRD, and steric sea-level change combined and for each basin using the reconstructed sea-level rolling trend at the nearest model grid cell to each tide gauge location. The tide gauge relative sea level is corrected for glacial isostatic adjustment (GIA), but we do not correct for contemporary GRD-induced or other sources of

contemporary vertical land movement (VLM) because of the limited number of tide gauges with co-located and bench-marked GNSS sites, instead removing the mean trend from tide gauge observed data. Rolling trends from observation data are treated identically as from model data: a seasonal signal is solved for within the regression design matrix (an annual and a semi-annual periodic) and the noise is assumed to have an AR(1) characteristic.

3 Data

3.1 High-resolution 58-year ocean model run: NEMO

The total sea-level signal is partitioned into steric and manometric sea level from the NEMO ORCA0083-N006 model run, details of which can be found in Marzocchi et al. (2015) and Moat et al. (2016). The model is applied to a high-resolution ORCA tripole grid (nominally 1/12°) and is eddy-resolving; it incorporates a sea-ice model and is forced by the Drakkar Surface Forcing data set version 5.2 (Dussin et al., 2016) from 1958 to 2015 inclusive. This data set derives ocean model forcing variables from the ERA40 and ERA-Interim atmospheric data sets and includes freshwater fluxes (precipitation and snow). Freshwater runoff is added as seasonal cycles and does not exhibit inter-annual changes. Because of deficiencies in the freshwater forcing, a moderate relaxation of surface salinity to climatology is applied and a freshwater budget restoration is applied at time steps when a deficit is found (and only applied to areas with precipitation).

Steric sea level is calculated using the TEOS-10 equation of state (TEOS-10, 2008) applied to temperature and salinity modelled values at each model depth level. The total and steric sea-level anomaly are affected by the Boussinesq approximation in this model setup (Greatbatch, 1994; Griffies and Greatbatch, 2012). This effect and the global ocean mean atmospheric pressure effect are removed by subtracting the global mean of each sea-level anomaly at each time step.

The manometric sea-level component is taken to be equal to the ocean bottom pressure anomaly, converted from pressure to millimetre change in height.

The ocean model has been shown to match observed variability well (Marzocchi et al., 2015). We additionally check that the linear trend from the last decade of the model run, 2005-2015, with GRD added matches the altimetry observation of the absolute sea-level trend (Supplement Fig. S1). In this analysis, only coastal locations within 25 km of the low-resolution GSHHG coastline are considered.

3.2 CMIP6 climate model historical runs

We ensure that sea-level trend variance given by the NEMO model is appropriate for our aim by checking that the variance magnitude lies within the envelope of sea-level trend variance from historically forced model runs from the 6th

Climate Model Intercomparison Program (CMIP6; Eyring et al., 2016).

Model run data were obtained via JASMIN (UK data and storage facility, https://jasmin.ac.uk/users/access/, last access: 22 August 2021) and may also be obtained from the WCRP portal (ESGF, 2021). Historical forcing (esm-hist) has been run in CMIP6 from 1850 to 2014 inclusive. Here we take the "zos" variable sea surface height monthly means from January 1958 until the end of the run in December 2014 (noting this is 1 year shorter than the high-resolution NEMO run). The "zos" variable is interpolated onto a regular lat–long $1/4°$ grid for each run and the global ocean mean is removed from each time step of each model. Appendix A lists the 43 CMIP6 model setups analysed in this study. In this analysis, only coastal locations within 25 km of the low-resolution GSHHG coastline are considered.

3.3 Climate mode and oceanographic indices

Major climate variability is represented by indices derived from various atmospheric and oceanic observables, such as air pressure at sea level, sea surface temperature, and surface wind speed or its gradient. Here, we determine the correlation of the principal component time series of rolling sea-level trends with the rolling trends of six major climate includes: the Pacific Decadal Oscillation (PDO; NOAA-NCEI, 2020c), El Niño–Southern Oscillation (ENSO; Multivariate ENSO Index, NOAA-NCEI, 2020a), North Atlantic Oscillation (NAO; NOAA-NCEI, 2020b), Arctic Oscillation (AO; NOAA-CPC, 2020), Southern Annular Mode (SAM; Marshall, 2020), and Indian Ocean Dipole (IOD; GCOS, 2020).

Additionally, the effect of the Atlantic Meridional Overturning Circulation (AMOC) is investigated. The AMOC index is calculated here from the NEMO model runs as an anomaly at each time step. The index is computed as the principal component of the low-pass-filtered (1-year running mean) and zonally integrated meridional transport (Sv), and then the rolling trend is calculated from this index.

It is acknowledged that these indices are not independent of each other. However, the EOF pattern and principal components of coastal sea-level change are orthogonal. Therefore, only one climate index is associated with each PC and not repeated in the reconstruction.

3.4 Absolute sea level: satellite altimetry

Absolute sea level is defined from the ESA SLCCI v2 multimission gridded product on a $1/4°$ grid with the most up-to-date corrections and processing available (Legeais et al., 2018; ESA, 2018). The standard global mean trend GIA correction is applied at each grid point ($-0.21\,\mathrm{mm\,yr^{-1}}$ for the ICE6G-VM_D GIA model, Peltier et al., 2015; Peltier, 2018). This global mean value represents the shift in geopotential surface of the geoid (Tamisiea, 2011). Because we are interested in the spatial distribution of sea-level trends,

the spatial redistribution of the geoid by GIA is also applied (Tamisiea, 2011) as a trend correction derived from the spherical harmonic coefficients provided by Peltier (2018). Contemporary GRD variability driven my mass redistribution affects the sea surface. Satellite altimetry observes spatial changes to the geoid from a centre of mass and should be corrected for the global mean volume change due to solid-Earth deformation (Frederikse et al., 2017). We correct the gridded satellite altimetry for solid-Earth deformation associated with recent mass loading of the oceans following Frederikse et al. (2020b) and using their published data (Frederikse et al., 2020a).

3.5 Tide gauge observations

Tide gauge observations are obtained from the Permanent Service for Mean Sea Level (Holgate et al., 2013) for revised local reference (RLR) stations only. The relative sea level is corrected for GIA (Peltier et al., 2015; Peltier, 2018) only, and no account is made for contemporary GRD-induced or other VLM. Because we are primarily interested in the temporal variability of sea-level trends associated with climate variability, in the figures we remove the time mean trend; the linear trend correction does not affect the results. Non-linear solid-Earth deformation from GRD and other sources such as ground compaction and building load are not accounted for and will be present in the tide gauge trend variability. Monthly mean time series, omitting flagged data, are used to determine rolling trends, and periods for which less than 50 % of data are missing in each rolling decade are omitted.

3.6 Gravitation, rotation, and solid-Earth deformation changes

The ocean models do not include any GRD changes. Observations by their nature include GRD effects. The solid-Earth deformation changes modify the basin shape and therefore global volume. For absolute sea level observed by satellite altimetry the global ocean mean solid-Earth deformation from contemporary mass redistribution and global mean glacial isostatic adjustment (GIA) effects are usually subtracted as a correction. Altimetry observes regional redistribution of the geoid when the anomalies are taken from a mean sea surface. Relative sea level observed by tide gauges includes solid-Earth deformation. To compare model data with observations, we add variability from a sea-level fingerprint method applied to comprehensive data sets of land and cryospheric mass loading. The data set has been used to estimate the GRD effect on global mean and basin mean sea-level trends with the time-varying vertical land movement used to correct tide gauge relative sea-level records (Frederikse et al., 2020a, b). The GRD geoid fingerprints include the effect of mass changes in glaciers as well as the Greenland and Antarctic ice sheets, including uncharted glaciers and peripheral glaciers, and from natural terres-

trial water storage (TWS), dam retention (or reservoir impoundment), and groundwater depletion. Here, we determine decadal rolling trends from the geoid variability of the sea-level fingerprint since 1958 and ignore the barystatic (global mean) component since we are interested in the spatial variability.

4 Results and discussion

4.1 Variance of decadal sea-level trend

Over the 58-year NEMO model run, coastal sea-level rolling trends vary in time by a mean standard deviation of $3.6\,\mathrm{mm\,yr^{-1}}$, with some locations displaying a standard deviation in trends over $7.5\,\mathrm{mm\,yr^{-1}}$ (Fig. 1), which is significantly larger then the mean trend over the modelled period of $2.2\,\mathrm{mm\,yr^{-1}}$.

The variance of total SSH in the NEMO model run generally sits within the spread of variance in the CMIP6 ensemble. There is increased variance in the CMIP6 ensemble mean compared with the NEMO model run in the Northern Hemisphere, particularly in the Beaufort Strait, Hudson Bay, and the North Sea into the Baltic Sea and to a lesser extent in the Mediterranean Sea and Black Sea (comparing Fig. 1a and b). It is well known that many coarse-resolution climate models do not reproduce sea level in semi-enclosed seas well because of resolution limits on fluxes with the ocean basins (Adloff et al., 2018; Meyssignac et al., 2017). In contrast, the NEMO model run displays a larger variance in sea-level trends around the coast of Greenland, in the tropical western Pacific and west coast of Australia, in the Caribbean Sea, and around Chesapeake Bay. However, most of these differences lie within the CMIP6 ensemble spread and are therefore not significant.

This analysis confirms there is high variability in decadal sea-level trend in the western tropical Pacific Ocean. On the eastern side where the coast faces the open ocean, the signal is dominated by steric changes, but through the Indonesian throughflow and in the marginal seas, the signal becomes manometric in nature (Fig. 2a, b). For most of the coastal locations, the variance in sea-level trend is dominated by manometric sea-level change; in 48.2 % of coastal locations defined from the NEMO grid the manometric sea-level change shows the largest contribution to variance, in 32.3 % of locations steric sea level is dominant, and in 17.5 % of locations the GRD effect is dominant.

Around the Greenland coast, in the vicinity of major ice mass loss that is variable in time, there is a large variability in decadal trends due to the GRD effect (Fig. 2c). The GRD signal driven by glacier and ice sheet mass loss also contributes more than one-quarter to the variability around southern Alaska, Hudson Bay, the Canadian Arctic, Iceland, and to a lesser extent around the Patagonian ice sheet. It is noted that this analysis relates to absolute sea-level equiva-

lent, and VLM contributing to relative sea level is not considered. There is also a notable contribution from GRD in areas around the major river basins or other hydrology impacts (like groundwater abstraction or dam retention) where inter-annual variability in TWS is large, for example around the Amazon River basin, Niger River basin, and the Persian Gulf.

Even though in many of those regions the variability in the decadal trend around the global mean is small (around $1\,\mathrm{mm\,yr^{-1}}$), where the dominant contributions are GRD and/or local steric contributions from hydrology, future changes may exacerbate the trend. For example, in the Persian Gulf, decadal sea-level trends are dominantly affected by GRD changes over direct oceanographic changes in addition to global mean sea-level rise. It is noted here that there is a complex GRD signal from both hydrology and glacier mass loss. On the south-eastern African coast, as in much of the South Atlantic, where there are very few long-duration tide gauge measurements, the trend variability is small (less than $1\,\mathrm{mm\,yr^{-1}}$) in both the CMIP6 ensemble mean and NEMO model (Fig. 1a,b). Here, sea-level variability is strongly influenced by GRD effects from the variability of hydrology, with the Amazon, Niger, Congo, and Zambezi–Okavango basins driving more than 40 % of sea-level trend variability in places (Fig. 2c). Long-term anthropogenic or climate change impacts on the hydrology in these locations are likely to intensify the regional trend about the global mean.

4.2 Climate index reconstruction of sea-level trends

We reconstruct decadal running sea-level trends from climate index trends by ocean basin for steric and manometric sea level separately and then combine the reconstructions. When compared with the NEMO model sea-level rolling trends at each coastal grid point (from which the regression coefficients were derived), the reconstruction displays statistically significant correlations ($r > 0.32$ for a two-sided t test at the 95 % confidence interval with an auto-correlation of 0.5 in the rolling trends) along much of the global coastal locations (Fig. 3a). There is a notably poor correlation around south-eastern Africa, where the interaction of the Benguela and Agulhas currents as well as upwelling may interrupt far-field climate-driven sea-level variability. The proportion of sea-level trend variance reconstructed by climate variability through our approach is small around much of the global coast (orange, grey, pink in Fig. 3). The reconstruction explains more than half of the decadal sea-level variance along the American continent's west coast, in the tropical Pacific Ocean, and in the Indonesian throughflow to the western Australian coast and west coast of Asia (blue in Fig. 3b). The primary mode explains more than half of the decadal trend variance in the semi-enclosed seas of the eastern Mediterranean, Black, and Baltic seas. Along the traditionally under-sampled West African coastline between $10°\,\mathrm{N}$ and the Mediterranean outflow at the Strait of
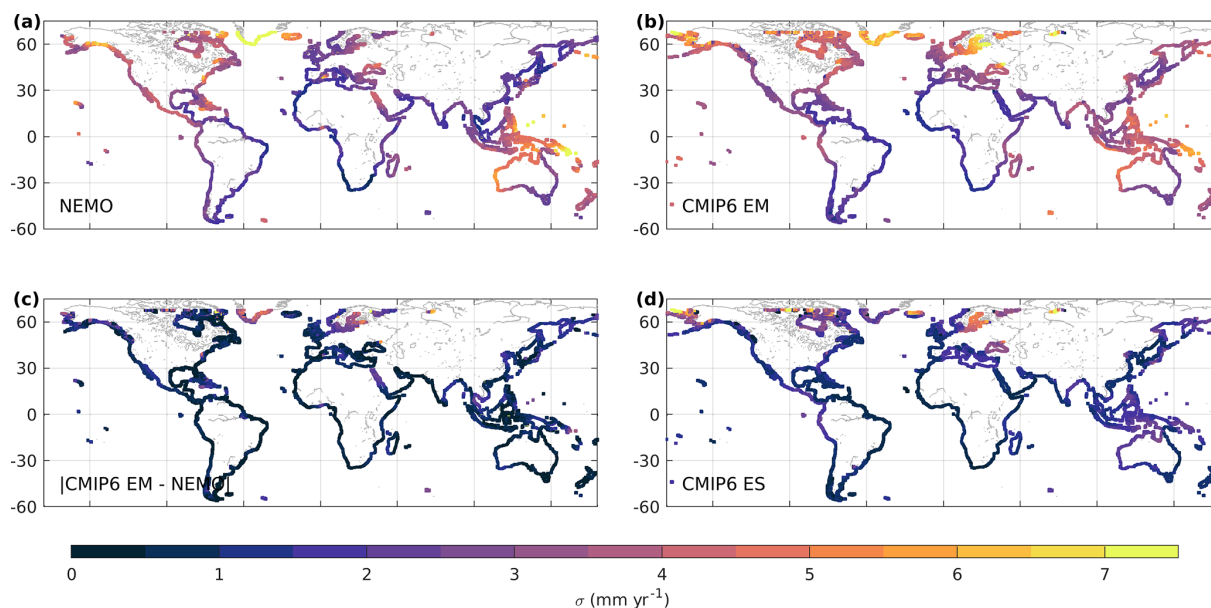
Figure 1. Comparison of the variability in decadal sea-level trends between NEMO and an ensemble of CMIP6 model runs. The standard deviation of decadal trends (mm yr^{-1}) in sea surface height from the NEMO model (**a**), the ensemble mean EM of the CMIP6 model runs (**b**), and the absolute difference between NEMO and CMIP6 EM (**c**), which may be compared against the CMIP6 ensemble spread: ES (**d**). The SSH from the NEMO model and ensemble mean of CMIP6 model runs (**a, b**) include GRD.

Gibraltar as well as between 5 and 30° S, the reconstruction explains between one-third and one-half of variability in decadal trends. The approach explains more than half of decadal trend variance over 25.8 % of the global, non-polar coastal ocean and with greater success in the Pacific Ocean where the ENSO variability is dominant (Table 1). Table 1 presents the proportion of grid cells located in each basin where the reconstruction explains more than one-third, one-half, or two-thirds of the decadal sea-level trend variance (not area-averaged). The column "SSH" refers to a reconstruction using only total SSH EOFs, and the column "DSL + steric" refers to a reconstruction summed from the EOFs of all sea-level components. For each major basin, the approach can explain more than one-third of the decadal trend variance for 24.6 % to 73.1 % of coastal locations (Table 1).

When considering the proportion of variance explained for a coastal location, the manometric sea-level signal becomes important. The first principal component modes from manometric and steric sea level are very similar to that from sea surface height and have the highest correlation with the same climate indices, except for the influence of AMOC in the Atlantic Ocean (Supplement Table S1 and Figs. S5 and S11). However, by adding the contribution from each component separately there is a marginal improvement in the overall variance explained by this approach (Table 1). Splitting the variance into component parts allows the EOF analysis to determine more specific spatial patterns for each component part, whereas the total SSH is dominated by different physical processes in different areas (Fig. 2).

Oscillations in observed tide gauge decadal trends are explained well by the climate index reconstruction in some regions, in particular across the tropical Pacific and the coast of the Americas as well as on the Atlantic west coast (examples are given in Fig. 4). Where the majority of the signal is manometric, for example the west coast of Australia and the Gulf of Maine (Fig. 4c, e), coastally trapped waves propagate along the continental slope and shelf. Where the continental shelf is narrow, the reconstructed sea level is predominantly steric (Fig. 4b). In the tropical western Pacific, the dominant ENSO steric signal directly impacts tropical western Pacific tide gauge sites on the oceanward (eastern) coast, but the signal propagates through the Indonesian throughflow and around the island as a manometric signal, so by Cebu the signal is predominantly manometric (Fig. 4a). The tide gauge data do not have contemporary VLM removed (except GIA), nor the nodal tide or inverse barometer correction made. For visualisation we simply remove the mean trend for the whole period considered.

For locations with large-magnitude variability in the trend, i.e. with a standard deviation larger than the global mean trend of 3.5 mm yr^{-1} (orange and yellow is Fig. 1a, b), typically more than half of that decadal signal can be attributed to climate forcing and reconstructed from climate indices. For 10 % of the coastal locations in this study, over two-thirds of the regional decadal sea-level trend about the global mean can be quantified by a linear relationship with climate index data (Table 1).
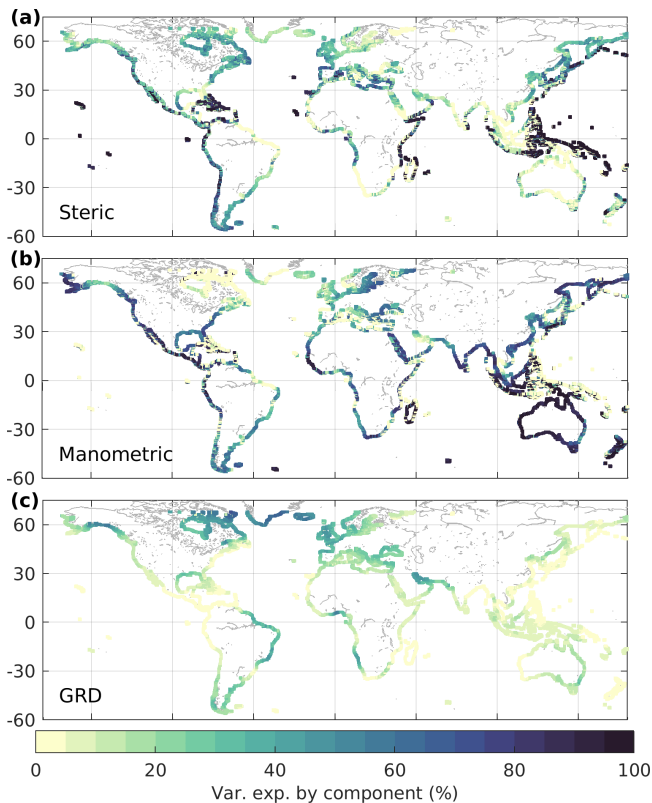
Figure 2. Proportion of variance explained (%) by sea-level components of the rolling decadal trends in sea surface height from the NEMO model by steric sea level (**a**), manometric sea level (**b**), and GRD, respectively (**c**). Figure 1a presents the magnitude of the variability (standard deviation).

4.3 Climate effect on recent coastal sea-level trends

The reconstructed sea-level variability due to primary climate modes can be compared against the spatially comprehensive satellite altimetry data, with the global mean trend removed (to emphasise regional patterns in sea-level change).

For a recent decade of observations, 2008–2018 inclusive, the reconstruction of the sea-level trend anomaly along the coast associated with climate indices (Fig. 5) captures the dipole of the sea-level trend anomaly across the Pacific Ocean and at least one-third of the decadal trend anomaly in the Caribbean Sea and Black Sea, as well as the sign of the trend anomaly in southern Greenland, the Baltic Sea, and the north-western African coast. The reconstructed signal is not as strong as observed. In some regions, such as the Gulf of Mexico, the reconstructed trend associated with climate variability (Fig. 5b) displays the opposite sign to the observed trend (Fig. 5a); in these locations in this period, the observed-minus-reconstructed trends have a larger-magnitude trend from the global mean. The histogram of trend anomalies for this period are markedly more Gaussian when reconstructed
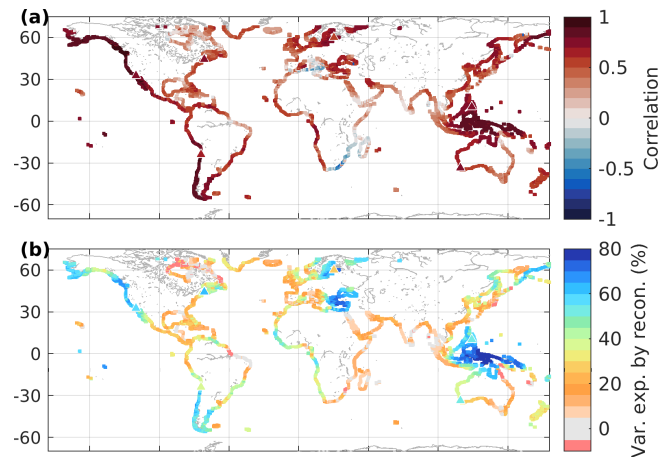

Figure 3. Comparison of decadal rolling sea-level trends from the NEMO model plus GRD, and reconstruction using only climate indices: Pearson's correlation coefficient (**a**) and variance explained (**b**; %). The results here sum the reconstructed decadal trend from manometric sea level plus steric sea level by ocean basin. Triangles denote the locations of tide gauge observations shown in Fig. 4.

with climate-index-related variability removed than the unaltered observations.

Notably in all basins, by removing the reconstructed variance by climate indices, the mean (median) coastal sea-level trend for 2008–2018 is increased by 0.7 (0.2) mm yr^{-1} globally (Table 2). It is noted that we expect climate variability has affected the global mean sea level over the same period, which we do not account for here, but we may conclude that coastal sea levels have been suppressed by the phase of climate variability in 2008–2018 compared with the entire ocean mean.

4.4 Sources of decadal variability and caveats

Inter-annual sea-level variability can develop purely as a response to non-linear interactions in oceanic intrinsic variability and can evolve from seasonal forcing as strongly as from atmospheric forcing (Llovel et al., 2018). Oceanic intrinsic variability exceeds the forced response to atmospheric forcing at some length scales over several years in high-resolution ensembles (Sérazin et al., 2015, 2016; Llovel et al., 2018; Penduff et al., 2019). Thus, sea-level variability is the aggregated response over integrating timescales of both atmospheric forcing and intrinsic variability in the system. It is acknowledged that the approach could be improved by comparing the PCs with phase-lagged trends in the climate indices and/or with other metrics describing the forcing.

Globally, the ENSO and PDO have been shown to dominate the decadal-scale variability of coastal sea level over other climate processes (e.g. Hamlington et al., 2013; Nerem et al., 2018). Because the PDO or ENSO decadal variability dominates the power in sea-level variability, the EOF bases
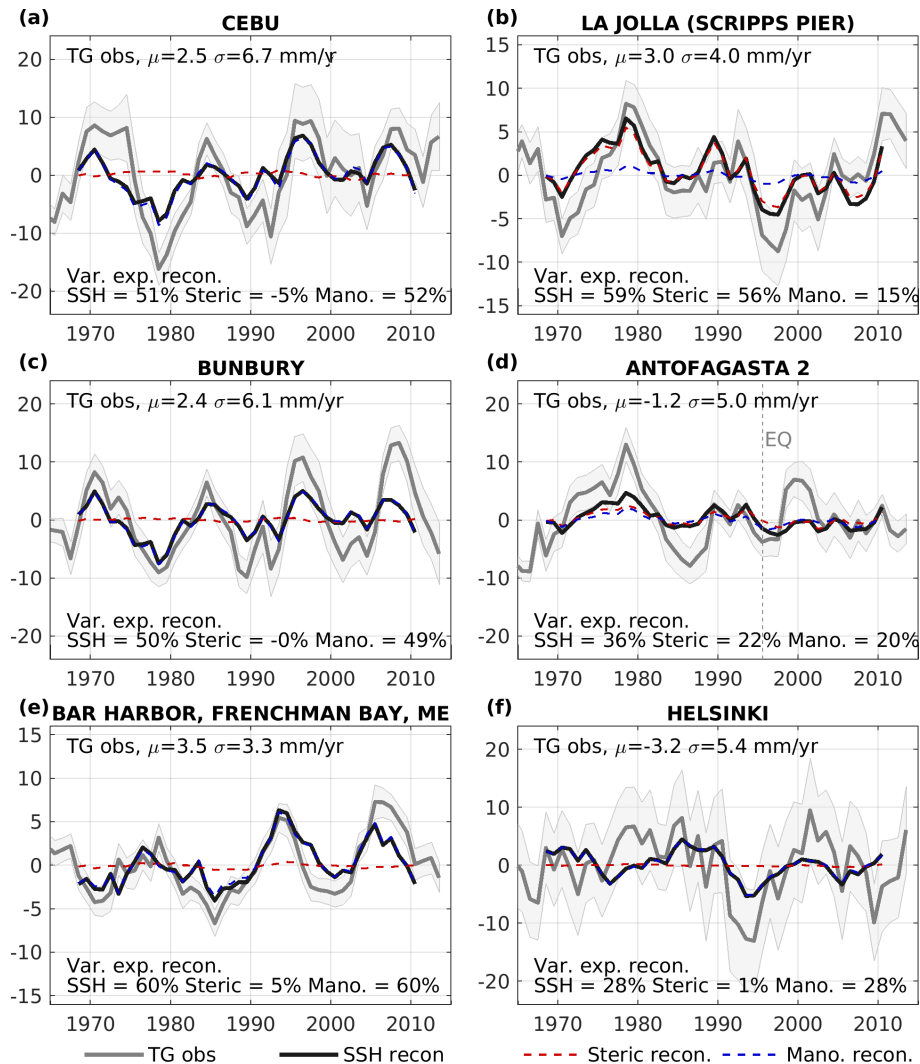
Figure 4. Observed sea-level trends in tide gauge observed sea level (mm yr^{-1}; grey solid lines, light grey shading presents 1σ trend error estimates, triangles in Fig. 3) and the reconstructed decadal trends from all PCs for the appropriate basin for steric sea level (red dashed), manometric plus GRD sea level (blue dashed), and the sum (black solid). Note that the time mean sea-level trend is removed from all tide gauge observed data for visualisation.

on a global data set are forced to be orthogonal to that mode. To investigate other drivers, we further mask the data into three oceanic basins: the Atlantic, Pacific, and Indian oceans. By focusing on each oceanic basin in turn, the dominant mode(s) from each region can be identified (Table 3; Supplement Table S1 and Figs. S4 to S18). Since we aim to reconstruct decadal-scale sea-level trends, it is difficult to make direct comparisons with previous studies of climate variability and sea-level change. The dominant influence of ENSO and PDO indices with Pacific and Indian Ocean sea level agrees with other works (e.g. Zhang and Church, 2012; Hamlington et al., 2019; Wang et al., 2021; Pfeffer et al., 2018, 2022). In the North Atlantic Ocean, our approach finds a stronger relationship between sea-level variability and AMOC, followed by the AO. Previous studies that include inter-annual vari-

ability find strong relationships with the NAO (Frederikse et al., 2018). Studies that separate the sea-level components have found that steric sea-level variability strongly relates to the Atlantic Multidecadal Oscillation (AMO) (Pfeffer et al., 2018), and our approach results in a similar relationship between manometric sea-level change and the AO as in Pfeffer et al. (2022) (Supplement Fig. S12).

Generally, climate models display lower sea-level variability than observed (Carson et al., 2015). In particular, the CMIP5 models were found to simulate sea-level variability comparable to observations but showed a bias in trends (Meyssignac et al., 2017); other authors found that the long-term memory, power-law character of sea level in CMIP5 models is too small, indicating the sea-level variability is too short-lived (Becker et al., 2016). Here, the use of a high-
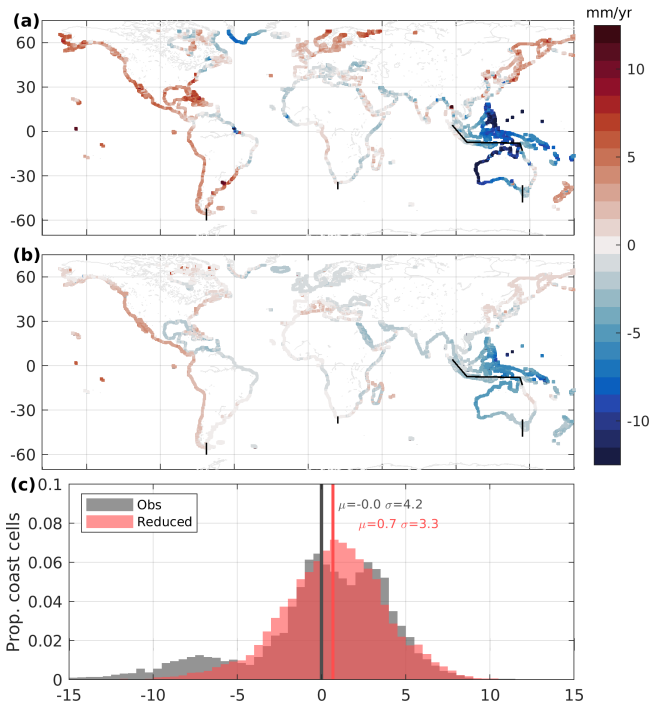
Figure 5. Comparison of 2008–2018 trend anomaly (mm yr^{-1}) from satellite altimetry and the reconstruction. The observed decadal trend in satellite altimetry with the global mean removed (**a**) and the reconstructed decadal trend for each basin and component combined (**b**), with a histogram (**c**) for all coastal grid cell locations for observations from satellite altimetry (grey) and the altimetry minus the reconstruction (so-called "reduced" trends, red).

resolution model goes some way to minimise that influence, but we caution that the resulting reconstructed sea-level variability and its trend should be thought of as a minimum rise or fall in sea level expected with climate index evolution.

It is acknowledged that the EOF patterns and their PCs developed here are somewhat model-dependent and because of the linear approach taken may incorporate anthropogenic as well as internal forcing patterns. Because of the multi-collinearity in the explanatory variables (climate mode indices) and auto-correlation in the variables, there are limitations on any type of regression analysis that attempts to associate climate variability with sea-level variability. The EOF analysis may split the variability from a given physical process into more than one mode, weakening the relationship with any single climate mode index. Therefore, the reconstructed climate-associated sea-level trends produced should be thought of as lower limits at each location of the trend variance about the mean trend. A multivariate approach with regularisation could be applied instead.

Table 1. The proportion of coastal grid cells defined from the NEMO grid with more than one-quarter (25 %), one-third (33 %), one-half (50 %), two-thirds (67 %), and three-quarters (75 %) of decadal trend variance explained by the reconstruction. The values shown here are from assessment of the "coastal domain" and the NEMO model runs. "SSH" refers to the reconstruction using EOF and PC modes for the full SSH signal, and "DSL + steric" refers to the reconstruction by component for manometric dynamic sea level, GRD, and steric sea level associated with climate indices separately and then summed.

Coastal domain	> Var. exp.	SSH	DSL + steric
All basins	one-quarter	58.9	54.9
	one-third	48.2	44.5
	one-half	29.3	25.8
	two-thirds	7.2	12.3
	three-quarters	1.8	5.7
Atlantic	one-quarter	52.4	40.8
	one-third	41.2	28.7
	one-half	21.4	8.7
	two-thirds	4.8	0.0
	three-quarters	0.1	0.0
Pacific	one-quarter	78.9	82.0
	one-third	66.9	73.1
	one-half	46.6	54.2
	two-thirds	12.7	32.8
	three-quarters	4.6	15.3
Indian	one-quarter	24.4	29.9
	one-third	19.6	24.6
	one-half	8.7	9.1
	two-thirds	0.3	0.0
	three-quarters	0.0	0.0

Table 2. Statistics of the global–coastal sea-level trend from 2008–2018 observed by satellite altimetry and when reduced by the reconstructed sea level expected from the climate index reconstruction for each basin (mm yr^{-1}).

Statistic	Coastal domain	Obs.	Reduced	Diff.
SD	Global	4.2	3.3	−1.0
	Atlantic	2.8	3.0	0.2
	Pacific	5.2	3.3	−1.9
	Indian	4.6	3.7	−1.0
Mean	Global	0.0	0.7	0.7
	Atlantic	0.8	1.1	0.3
	Pacific	−0.1	0.6	0.7
	Indian	−3.0	−1.0	2.0

5 Conclusions

The current temporal duration of high-quality sea-level data with good spatial coverage conflates with the typical auto-correlated, integrated, long-memory timescale of variabil-

Table 3. The linear trend coefficient between the decadal trend in the climate index and the first PC time series in each basin and for each component of sea level.

Component	Atlantic index	beta	Pacific index	beta	Indian index	beta
Steric PC1	AMOC	−0.83	ENSO	1.60	ENSO	−0.95
Manometric PC1	AMOC	−1.01	ENSO	1.64	ENSO	−1.24
GRD PC1	AMOC	−0.67	AMOC	−0.88	AMOC	−0.84

ity in major atmosphere–ocean climate modes, as recently shown for steric sea-level variability, particularly in the Atlantic by Pfeffer et al. (2018) and for the open Pacific Ocean by Hamlington et al. (2020a). Therefore, much of the current linear trend in steric and manometric components of sea level can be reconstructed from climate index data in some parts of the global coast. This enables the possibility that observed sea level and its components can be reduced for climate variability, as has been applied for the total sea-level signal at the global scale (Nerem et al., 2018; Hamlington et al., 2020c), spatial distribution in the Pacific Ocean (Hamlington et al., 2020a, b), and globally for time series (Wang et al., 2021).

We present an analysis of the variance in local, short-term (decadal) sea-level trends about the global mean around the Atlantic, Pacific, and Indian Ocean coastlines. These data are an indicative lower bound of uncertainty in regional short-term trend deviations from global mean projections. The standard deviation of decadal trend exceeds the global mean of $3.5\,\mathrm{mm\,yr^{-1}}$ along the eastern North Pacific, western tropical Pacific, New Zealand, and western Australian coastlines as well as the eastern Indian Ocean, parts of the Caribbean Sea coast and western Atlantic coastline including the Greenland coast, and many semi-enclosed seas.

For a recent decade of observations, from 2008–2018, the global–coastal mean sea level (here defined within 25 km of the coast and ignoring the Arctic and Antarctic coastlines) has been suppressed by climate variance by $0.7\,\mathrm{mm\,yr^{-1}}$ in the coastal mean. In particular, this increase is greatest in the Indian Ocean basin ($2.0\,\mathrm{mm\,yr^{-1}}$ greater).

More than half of the decadal sea-level trend can be explained by a linear regression with major climate index trends at around 25 % of global coastal (within 25 km of the coast) locations, rising to 54 % of grid cells around the Pacific Ocean. The ENSO and PDO variability dominates here, and the open-ocean variability observed by many previous studies extends to and around the coast, most notably in the western tropical Pacific and along the coast of the Americas. Our approach has no lag or lead time introduced and explains less than one-third of the decadal variance in the low-latitude eastern Pacific Ocean and in the mid-latitudes of the western Pacific. In the Indian Ocean, our method is most successful in the eastern basin, where the propagation of ENSO-related sea-level disturbance dominates through the Indonesian throughflow and therefore dominates the first

EOF mode, explaining more than 40 % of decadal variance along the western Australia coast but less than 20 % elsewhere. In the Atlantic Ocean our approach works well in the Baltic, Black, and eastern Mediterranean seas and along the west coast of North Africa (eastern tropical Atlantic Ocean), with more than 50 % variance explained in places, but is less informative on the north-eastern Atlantic margin. Notably, this region of North Africa and other regions where the variance explained is lower but still statistically significant, such as the Caribbean seas and Bay of Bengal, have a lack of good-quality and long-duration tide gauge data by which to evaluate the decadal-scale variability needed to make helpful forecasts of sea-level trends over the mid-term. The dominant influence of ENSO and PDO on sea-level change in the Pacific and Indian Ocean and the influence of AO on Atlantic Ocean manometric sea-level change match previous studies (Zhang and Church, 2012; Hamlington et al., 2019; Wang et al., 2021; Pfeffer et al., 2022). Our approach finds a strong relationship between AMOC and decadal sea-level change in all basins.

The variability of GRD in the total sea-level trend should not be ignored over timescales of the order of 10 years (Fig. 2). The variability in decadal-scale coastal sea-level trends over much of the coastal ocean is dominated by manometric and GRD sea-level components rather than steric sea level. The coasts where steric sea-level trend variability dominates the signal are mostly tropical or low-latitude towards the west of ocean basins and at the oceanic extent of the continental shelf. Sea-level disturbances that originate as steric in the open ocean propagate onto the continental shelf as a mass signal at the local scale. Thus, sea-level trends in the open ocean that can be associated with steric forcing need to be propagated accordingly onto the shelf, i.e. using high-resolution models, to adequately forecast variability at the coast. Future anthropogenic or climate change influences on hydrology- and ice-mass-change-driven GRD will disproportionately affect some regions that historically display low decadal variance, such as the Amazon Basin, the west coast of Africa from Niger, Congo, and Zambezi hydrology, and the Persian Gulf.

Appendix A: CMIP6 models

The CMIP6 models used in this study are given in Table A1.

Table A1. List of CMIP6 models used in this study.

Model name	Model centre	Resolution
ACCESS-CM2	CSIRO-ARCCSS	–
ACCESS-ESM1-5	CSIRO	–
BCC-CSM2	BCC	MR
CAMS-CSM1-0	CAMS	–
CanESM5	CCCma	–
CAS-ESM2-0	CAS	–
CESM2	NCAR	–
CESM2-FV2	NCAR	–
CESM2-WACCM	NCAR	–
CESM2-WACCM-FV2	NCAR	–
CIESM	THU	–
CMCC-CM2	CMCC	HR4
CMCC-CM2	CMCC	SR5
E3SM-1-0	USDOE	–
E3SM-1-1	USDOE	–
E3SM-1-1-ECA	USDOE	–
EC-Earth3	EC-Earth-Consortium	–
EC-Earth3-AerChem	EC-Earth-Consortium	–
EC-Earth3-Veg	EC-Earth-Consortium	–
EC-Earth3-Veg	EC-Earth-Consortium	LR
FGOALS-f3-L	CAS	–
FGOALS-g3	CAS	–
FIO-ESM-2-0	FIO	–
GFDL-CM4	GFDL	–
GFDL-ESM4	GFDL	–
GISS-E2-1-G	NASA-GISS	–
GISS-E2-1-G-CC	NASA-GISS	–
GISS-E2-1-H	NASA-GISS	–
INM-CM4-8	INM	–
INM-CM5-0	INM	–
IPSL-CM6A	IPSL	LR
KIOST-ESM	KIOST	–
MIROC6	MIROC	–
MPI-ESM-1-2-HAM	HAMMOZ-Consortium	–
MPI-ESM1-2	MPI-M	LR
MPI-ESM1-2	MPI-M DWD DKRZ	HR
MRI-ESM2-0	MRI	–
NESM3	NUIST	–
NorCPM1	NCC	–
NorESM2	NCC	LM
NorESM2	NCC	MM
SAM0-UNICON	SNU	–
TaiESM1	AST	–

References

Adloff, F., Jordà, G., Somot, S., Sevault, F., Arsouze, T., Meyssignac, B., Li, L., and Serge, P.: Improving sea level simulation in Mediterranean regional climate models, Clim. Dy-

nam., 51, 1167–1178, https://doi.org/10.1007/s00382-017-3842-3, 2018.

Becker, M., Karpytchev, M., Marcos, M., Jevrejeva, S., and Lennartz-Sassinek, S.: Do climate models reproduce complexity of observed sea level changes?, Geophys. Res. Lett., 43, 5176–5184, https://doi.org/10.1002/2016GL068971, 2016.

Bingham, R. J. and Hughes, C. W.: Local diagnostics to estimate density-induced sea level variations over topography and along coastlines, J. Geophys. Res.-Ocean., 117, C01013, https://doi.org/10.1029/2011JC007276, 2012.

Bos, M. S., Fernandes, R. M. S., Williams, S. D. P., and Bastos, L.: Fast error analysis of continuous GNSS observations with missing data, J. Geodesy, 87, 351–360, https://doi.org/10.1007/s00190-012-0605-0, 2013.

Carson, M., Köhl, A., and Stammer, D.: The Impact of Regional Multidecadal and Century-Scale Internal Climate Variability on Sea Level Trends in CMIP5 Models, J. Clim., 28, 853–861, https://doi.org/10.1175/JCLI-D-14-00359.1, 2015.

Carson, M., Lyu, K., Richter, K., Becker, M., Domingues, C. M., Han, W., and Zanna, L.: Climate Model Uncertainty and Trend Detection in Regional Sea Level Projections: A Review, Surv. Geophys., 40, 1631–1653, https://doi.org/10.1007/s10712-019-09559-3, 2019.

Coward, A. C.: Archive data from run 6 of the NEMO 1/12° global ocean model, NCAS British Atmospheric Data Centre [data set], https://gws-access.ceda.ac.uk/public/nemo/runs/ORCA0083-N06/means/ (last access: 23 October 2019), 2016.

Dangendorf, S., Rybski, D., Mudersbach, C., Müller, A., Kaufmann, E., Zorita, E., and Jensen, J.: Evidence for long-term memory in sea level, Geophys. Res. Lett., 41, 5530–5537, https://doi.org/10.1002/2014GL060538, 2014.

Dussin, R., Barnier, B., and Brodeau, L.: The making of Drakkar forcing set DFS5, Tech. rep., LGGE, DRAKKAR/MyOcean Report 01-04-16, 2016.

Emery, W. J. and Thomson, R. E.: Data Analysis Methods in Physical Oceanography, Elsevier Science, Elsevier, https://doi.org/10.1016/C2010-0-66362-0, 2001.

ESA: Time series of gridded Sea Level Anomalies, CCI Open Data Portal [data set], https://doi.org/10.5270/esa-sea_level_cci-MSLA-1993_2015-v_2.0-201612, 2018.

ESGF: WCRP Coupled Model Intercomparison Project (Phase 6) data portal, https://esgf-index1.ceda.ac.uk/search/cmip6-ceda/, last access: 22 August 2021.

Eyring, V., Bony, S., Meehl, G. A., Senior, C. A., Stevens, B., Stouffer, R. J., and Taylor, K. E.: Overview of the Coupled Model Intercomparison Project Phase 6 (CMIP6) experimental design and organization, Geosci. Model Dev., 9, 1937–1958, https://doi.org/10.5194/gmd-9-1937-2016, 2016.

Fasullo, J. T. and Nerem, R. S.: Altimeter-era emergence of the patterns of forced sea-level rise in climate models and implications for the future, P. Natl. Acad. Sci. USA, 115, 12944–12949, https://doi.org/10.1073/pnas.1813233115, 2018.

Fasullo, J. T., Gent, P. R., and Nerem, R. S.: Forced Patterns of Sea Level Rise in the Community Earth System Model Large Ensemble From 1920 to 2100, J. Geophys. Res.-Ocean., 125, e2019JC016030, https://doi.org/10.1029/2019JC016030, 2020.

Frankcombe, L. M., McGregor, S., and England, M. H.: Robustness of the modes of Indo-Pacific sea level variability, Clim. Dy-

nam., 45, 1281–1298, https://doi.org/10.1007/s00382-014-2377-0, 2015.

Frederikse, T., Riva, R. E. M., and King, M. A.: Ocean Bottom Deformation Due To Present-Day Mass Redistribution and Its Impact on Sea Level Observations, Geophys. Res. Lett., 44, 12306–12314, https://doi.org/10.1002/2017GL075419, 2017.

Frederikse, T., Jevrejeva, S., Riva, R. E. M., and Dangendorf, S.: A Consistent Sea-Level Reconstruction and Its Budget on Basin and Global Scales over 1958–2014, J. Clim., 31, 1267–1280, https://doi.org/10.1175/JCLI-D-17-0502.1, 2018.

Frederikse, T., Landerer, F., Caron, L., Adhikari, S., Parkes, D., Humphrey, V. W., Dangendorf, S., Hogarth, P., Zanna, L., Cheng, L., and Wu, Y.-H.: The causes of sea-level rise since 1900, Zenodo [data set], https://doi.org/10.5281/zenodo.3862995, 2020a.

Frederikse, T., Landerer, F., Caron, L., Adhikari, S., Parkes, D., Humphrye, V. W., Dangendorf, S., Hogarth, P., Zanna, L., Cheng, L., and Wu, Y.-H.: The causes of sea-level rise since 1900, Nature, 54, 393–397, https://doi.org/10.1038/s41586-020-2591-3, 2020b.

GCOS: GCOS Dipole Mode Index (DMI), NOAA [data set], https://psl.noaa.gov/gcos_wgsp/Timeseries/DMI/, last access: 2 November 2020.

Greatbatch, R. J.: A note on the representation of steric sea level in models that conserve volume rather than mass, J. Geophys. Res., 99, 12 767–12 771, 1994.

Gregory, J. M., Griffies, S. M., Hughes, C. W., Lowe, J. A., Church, J. A., Fukumori, I., Gomez, N., Kopp, R. E., Landerer, F., Cozannet, G. L., Ponte, R. M., Stammer, D., Tamisiea, M. E., and van de Wal, R. S. W.: Concepts and Terminology for Sea Level: Mean, Variability and Change, Both Local and Global, Surv. Geophys., 40, 1251–1289, https://doi.org/10.1007/s10712-019-09525-z, 2019.

Griffies, S. M. and Greatbatch, R. J.: Physical processes that impact the evolution of global mean sea level in ocean climate models, Ocean Modell., 51, 37–72, https://doi.org/10.1016/j.ocemod.2012.04.003, 2012.

Haigh, I. D., Wahl, T., Rohling, E. J., Price, R. M., Pattiaratchi, C. B., Calafat, F. M., and Dangendorf, S.: Timescales for detecting a significant acceleration in sea level rise, Nat. Commun., 5, 3635, https://doi.org/10.1038/ncomms4635, 2014.

Hamlington, B. D., Leben, R. R., Strassburg, M. W., Nerem, R. S., and Kim, K.-Y.: Contribution of the Pacific Decadal Oscillation to global mean sea level trends, Geophys. Res. Lett., 40, 5171–5175, https://doi.org/10.1002/grl.50950, 2013.

Hamlington, B. D., Strassburg, M. W., Leben, R. R., Han, W., Nerem, R. S., and K-Y., K.: Uncovering the anthropogenic sea-level rise signal in the Pacific Ocean, Nat. Clim. Change, 4, 782–785, https://doi.org/10.1038/nclimate2307, 2014.

Hamlington, B. D., Fasullo, J. T., Nerem, R. S., Kim, K.-Y., and Landerer, F. W.: Uncovering the Pattern of Forced Sea Level Rise in the Satellite Altimeter Record, Geophys. Res. Lett., 46, 4844–4853, https://doi.org/10.1029/2018GL081386, 2019.

Hamlington, B. D., Frederikse, T., Thompson, P., Willis, J., Nerem, R., and Fasullo, J.: Past, Present and Future Pacific Sea Level-Change, Earth's Future, 8, 2020EF001839, https://doi.org/10.1029/2020EF001839, 2020a.

Hamlington, B. D., Frederikse, T., Nerem, R. S., Fasullo, J. T., and Adhikari, S.: Investigating the Acceleration of Regional Sea Level Rise During the Satellite Al-

timeter Era, Geophys. Res. Lett., 47, e2019GL086528, https://doi.org/10.1029/2019GL086528, 2020b.

Hamlington, B. D., Piecuch, C. G., Reager, J. T., Chandan-purkar, H., Frederikse, T., Nerem, R. S., Fasullo, J. T., and Cheon, S.-H.: Origin of interannual variability in global mean sea level, P. Natl. Acad. Sci. USA, 117, 13983–13990, https://doi.org/10.1073/pnas.1922190117, 2020c.

Holgate, S. J., Matthews, A., Woodworth, P. L., Rickards, L. J., Tamisiea, M. E., Bradshaw, E., Foden, P. R., Gordon, K. M., Jevrejeva, S., and Pugh, J.: New Data Systems and Products at the Permanent Service for Mean Sea Level, J. Coast. Res., 29, 493–504, https://doi.org/10.2112/JCOASTRES-D-12-00175.1, 2013.

IPCC: IPCC Special Report on the Ocean and Cryosphere in a Changing Climate, edited by: Po¨rtner, H.-O., Roberts, D. C., Masson-Delmotte, V., Zhai, P., Tignor, M., Poloczanska, E., Mintenbeck, K., Alegría, A., Nicolai, M., Okem, A., Petzold, J., Rama, B., and Weyer, N. M., Cambridge University Press, Cambridge, UK and New York, NY, USA, 755 pp., https://doi.org/10.1017/9781009157964, 2019.

Kleinherenbrink, M., Riva, R., and Sun, Y.: Sub-basin-scale sea level budgets from satellite altimetry, Argo floats and satellite gravimetry: a case study in the North Atlantic Ocean, Ocean Sci., 12, 1179–1203, https://doi.org/10.5194/os-12-1179-2016, 2016.

Landerer, F. W., Jungclaus, J. H., and Marotzke, J.: Regional Dynamic and Steric Sea Level Change in Response to the IPCC-A1B Scenario, J. Phys. Oceanogr., 37, 296–312, https://doi.org/10.1175/JPO3013.1, 2007.

Legeais, J.-F., Ablain, M., Zawadzki, L., Zuo, H., Johannessen, J. A., Scharffenberg, M. G., Fenoglio-Marc, L., Fernandes, M. J., Andersen, O. B., Rudenko, S., Cipollini, P., Quartly, G. D., Passaro, M., Cazenave, A., and Benveniste, J.: An improved and homogeneous altimeter sea level record from the ESA Climate Change Initiative, Earth Syst. Sci. Data, 10, 281–301, https://doi.org/10.5194/essd-10-281-2018, 2018.

Llovel, W., Penduff, T., Meyssignac, B., Molines, J.-M., Terray, L., Bessières, L., and Barnier, B.: Contributions of Atmospheric Forcing and Chaotic Ocean Variability to Regional Sea Level Trends Over 1993–2015, Geophys. Res. Lett., 45, 13405–13413, https://doi.org/10.1029/2018GL080838, 2018.

Marshall, G. J.: An observation-based Southern Hemisphere Annular Mode Index, British Antarctic Survey [data set], https://legacy.bas.ac.uk/met/gjma/sam.html, last access: 31 August 2020.

Marzocchi, A.-M., Hirschi, J. J., Holliday, N. P., Cunningham, S. A., Blaker, A. T., and Coward, A. C.: The North Atlantic subpolar circulation in an eddy-resolving global ocean model, J. Mar. Syst., 142, 126–143, https://doi.org/10.1016/j.jmarsys.2014.10.007, 2015.

Meyssignac, B., Slangen, A. B. A., Melet, A., Church, J. A., Fettweis, X., Marzeion, B., Agosta, C., Ligtenberg, S. R. M., Spada, G., Richter, K., Palmer, M. D., Roberts, C. D., and Champollion, N.: Evaluating Model Simulations of Twentieth-Century Sea-Level Rise, Part II: Regional Sea-Level Changes, J. Clim., 30, 8565–8593, https://doi.org/10.1175/JCLI-D-17-0112.1, 2017.

Moat, B. I., Josey, S. A., Sinha, B., Blaker, A. T., Smeed, D. A., McCarthy, G. D., Johns, W. E., Hirschi, J. J.-M., Frajka-Williams, E., Rayner, D., Duchez, A., and Coward, A. C.: Major variations in subtropical North Atlantic heat transport at short (5 day)

timescales and their causes, J. Geophys. Res.-Ocean., 121, 3237–3249, https://doi.org/10.1002/2016JC011660, 2016.

Nerem, R. S., Beckley, B. D., Fasullo, J. T., Hamlington, B. D., Masters, D., and Mitchum, G. T.: Climate-change – driven accelerated sea-level rise detected in the altimeter era, P. Natl. Acad. Sci. USA, 115, 2022–2025, https://doi.org/10.1073/pnas.1717312115, 2018.

Nidheesh, A., Lengaigne, M., and Vialard, J.: Natural decadal sea-level variability in the Indian Ocean: lessons from CMIP models, Clim. Dynam., 53, 5653–5673, https://doi.org/10.1007/s00382-019-04885-z, 2019.

NOAA-CPC: NOAA-CPC Arctic Oscillation Index (AO), NOAA [data set], https://www.cpc.ncep.noaa.gov/products/precip/CWlink/daily_ao_index/ao_index.html, last access: 2 November 2020.

NOAA-NCEI: NOAA-ESRL PSL Multivariate ENSO Index (MEI), NOAA [data set], https://www.psl.noaa.gov/enso/mei.old/, last access: 31 August 2020a.

NOAA-NCEI: NCEI North Atlantic Oscillation (NAO) index, NOAA [data set], https://www.ncdc.noaa.gov/teleconnections/nao/, last access: 31 August 2020b.

NOAA-NCEI: NCEI Pacific Decadal Oscillation (PDO)index, NOAA [data set], https://www.ncdc.noaa.gov/teleconnections/pdo/, last access 27 February 2020c.

Peltier, W. R.: Stokes coefficients for the ICE-6G_C/D VM5a GIA forward model, https://www.atmosp.physics.utoronto.ca/~peltier/data.php, last access: 23 July 2018.

Peltier, W. R., Argus, D. F., and Drummond, R.: Space geodesy constrains ice age terminal deglaciation: The global ICE-6G_C (VM5a) model, J. Geophys. Res.-Sol. Ear., 120, 450–487, https://doi.org/10.1002/2014JB011176, 2015.

Penduff, T., Llovel, W., Close, S., Garcia-Gomez, I., and Leroux, S.: Processing Choices Affect Ocean Mass Estimates From GRACE, J. Geophys. Res.-Ocean., 124, 1029–1044, https://doi.org/10.1029/2018JC014341, 2019.

Peyser, C. E., Yin, J., Landerer, F. W., and Cole, J. E.: Pacific sea level rise patterns and global surface temperature variability, Geophys. Res. Lett., 43, 8662–8669, https://doi.org/10.1002/2016GL069401, 2016.

Pfeffer, J., Tregoning, P., Purcell, A., and Sambridge, M.: Multitechnique Assessment of the Interannual to Multidecadal Variability in Steric Sea Levels: A Comparative Analysis of Climate Mode Fingerprints, J. Clim., 31, 7583–7597, https://doi.org/10.1175/JCLI-D-17-0679.1, 2018.

Pfeffer, J., Cazenave, A., and Barnoud, A.: Analysis of the interannual variability in satellite gravity solutions: detection of climate modes fingerprints in water mass displacements across continents and oceans, Clim. Dynam., 58, 1065–1084, https://doi.org/10.1007/s00382-021-05953-z, 2022.

Richter, K., Meyssignac, B., Slangen, A. B. A., Melet, A., Church, J. A., Fettweis, X., Marzeion, B., Agosta, C., Ligtenberg, S. R. M., Spada, G., Palmer, M. D., Roberts, C. D., and Champollion, N.: Detecting a forced signal in satellite-era sea-level change, Environ. Res. Lett., 15, 094079, https://doi.org/10.1088/1748-9326/ab986e, 2020.

Royston, S., Bingham, R. J., and, Bamber, J. L.: Attributing decadal climate variability in coastal sea-level trends, Zenodo [data set], https://doi.org/10.5281/zenodo.5849268, 2022.

Sérazin, G., Penduff, T., Grégorio, S., Barnier, B., Molines, J.-M., and Terray, L.: Intrinsic Variability of Sea Level from Global Ocean Simulations: Spatiotemporal Scales, J. Clim., 28, 4279–4292, https://doi.org/10.1175/JCLI-D-14-00554.1, 2015.

Sérazin, G., Meyssignac, B., Penduff, T., Terray, L., Barnier, B., and Molines, J.-M.: Quantifying uncertainties on regional sea level change induced by multidecadal intrinsic oceanic variability, Geophys. Res. Lett., 43, 8151–8159, https://doi.org/10.1002/2016GL069273, 2016.

Tamisiea, M. E.: Ongoing glacial isostatic contributions to observations of sea level change, Geophys. J. Int., 186, 1036–1044, https://doi.org/10.1111/j.1365-246X.2011.05116.x, 2011.

TEOS-10: Release on the IAPWS Formulation 2008 for the Thermodynamic Properties of Seawater, IAPWS, Tech. Rep., R13-08, http://www.teos-10.org (last access: 16 April 2019), 2008.

Wada, Y., Reager, J., Chao, B., Wang, J., Lo, M.-H., Song, C., Li, Y., and Gardner, A. S.: Recent Changes in Land Water Storage and its Contribution to Sea Level Variations, Surv. Geophys., 38, 131–152, https://doi.org/10.1007/s10712-016-9399-6, 2017.

Wang, J., Church, J. A., and Zhang, X.: Reconciling global mean and regional sea level change in projections and observations, Nat. Commun., 12, 990, https://doi.org/10.1038/s41467-021-21265-6, 2021.

Woodworth, P. L., Melet, A., Marcos, M., Ray, R. D., Wöppelmann, G., Sasaki, Y. N., Cirano, M., Hibbert, A., Huthnance, J. M., Monserrat, S., and Merrifield, M. A.: Forcing Factors Affecting Sea Level Changes at the Coast, Surv. Geophys., 40, 1351–1397, https://doi.org/10.1007/s10712-019-09531-1, 2019.

Yin, J., Griffies, S. M., and Stouffer, R. J.: Spatial Variability of Sea Level Rise in Twenty-First Century Projections, J. Clim., 23, 4585–4607, https://doi.org/10.1175/2010JCLI3533.1, 2010.

Zhang, X. and Church, J. A.: Sea level trends, interannual and decadal variability in the Pacific Ocean, Geophys. Res. Lett., 39, l21701, https://doi.org/10.1029/2012GL053240, 2012.